

Short Papers

Three-Dimensional Blind Deconvolution of SPECT Images

Max Mignotte* and Jean Meunier

Abstract—Thanks to its ability to yield functionally rather than anatomically-based information, the three-dimensional (3-D) SPECT imagery technique has become a great help in the diagnostic of cerebrovascular diseases. Nevertheless, due to the imaging process, the 3-D single photon emission computed tomography (SPECT) images are very blurred and, consequently, their interpretation by the clinician is often difficult and subjective. In order to improve the resolution of these 3-D images and then to facilitate their interpretation, we propose herein to extend a recent image blind deconvolution technique (called the nonnegativity support constraint–recursive inverse filtering deconvolution method) in order to improve both the spatial and the interslice resolution of SPECT volumes. This technique requires a preliminary step in order to find the support of the object to be restored. In this paper, we propose to solve this problem with an unsupervised 3-D Markovian segmentation technique. This method has been successfully tested on numerous real and simulated brain SPECT volumes, yielding very promising restoration results.

Index Terms—Image restoration, Markov random field (MRF) model, single photon emission computed tomography (SPECT) imagery, three-dimensional (3-D) blind deconvolution, unsupervised segmentation.

I. INTRODUCTION

THREE-DIMENSIONAL SPECT images are obtained by the detection of radiations (gamma rays) coming from radioactive isotopes injected in the human body. Contrary to other medical imaging techniques, such as X-ray, computed tomography (CT), magnetic resonance imaging (MRI), etc., this imagery process is able to give functionally rather than anatomically-based information, such as the 3-D metabolic behavior of human brain, by visualizing the level of blood flow of a set of cross-sectional images. This study of regional cerebral blood flow (rCBF) can aid in the diagnostic of cerebrovascular diseases (e.g., Alzheimer's disease, Parkinson's disease, etc.) by indicating lower, or abnormal higher, 3-D metabolic activity in some brain regions.

Due to the imaging process, SPECT suffers from poor spatial resolution mainly owing to the 3-D scattering of the emitted photons. Consequently, resulting 3-D SPECT images are blurred and their interpretation by the nuclear physician is often difficult and subjective. If the object to be visualized is small compared to the source-to-collimator distance, this degradation phenomenon may be considered to be shift-invariant [1] and, neglecting noise, this one can be modeled by a 3-D convolution process between the true undistorted 3-D image and

the transfer function of the imaging system (also called the point spread function or PSF).

In order to improve the spatial resolution of SPECT volumes, some authors have, thus, investigated the SPECT image deblurring problem by neglecting the interslice blur and by approximating this transfer function with a two-dimensional (2-D) symmetric Gaussian function [2], [3], or by considering an *a priori* known PSF [4]. In this context, classical Wiener filter techniques [1], [2] or maximum entropy filter-based deconvolution technique [4] have then been proposed to achieve this deconvolution procedure and significant resolution improvements have been noticed [1], [2], [4]. Nevertheless, let us note that these methods don't take into account the interslice blur inherent to this 3-D SPECT imagery process and are sensitive to the assumption made on the nature of the blurring function. In our applications where little is known about the PSF, it can turn out to be more relevant to estimate directly the PSF from the observed input image. This problem of simultaneously estimating the PSF (or its inverse) and restoring an unknown image is called a "blind deconvolution" problem. Recent 2-D deconvolution techniques exist, such as nonnegativity support constraint–recursive inverse filtering (NAS–RIF) algorithm, and can also be efficiently extended in the 3-D SPECT imagery context. These techniques require to find, in a preliminary step, the support of the object to be restored. In this paper, we propose to solve this problem thanks to an unsupervised 3-D Markovian segmentation technique.

This paper is organized as follows. Section II briefly describes the proposed 3-D extension of the NAS–RIF deconvolution technique. In Section III, we detail the 3-D unsupervised Markovian segmentation algorithm allowing to find the exact support of the object to be restored. Deconvolution experimental results on phantoms, synthetic and real brain SPECT volumes are given in Section IV. Finally, we conclude in Section V.

II. 3-D DECONVOLUTION METHOD

A. Introduction

In our application, the degradation of a 3-D SPECT image (i.e., a SPECT volume) can be represented as the result of a convolution of the true SPECT volume with a 3-D blurring function (the PSF), plus an additive term to model the noise from the physical system. If the imaging system is assumed to be linear and shift invariant, this degradation process can then be expressed by the following linear model:

$$g(x, y, z) = f(x, y, z) * h(x, y, z) + n(x, y, z)$$

where

- $g(x, y, z)$ the degraded or blurred 3-D image;
- $f(x, y, z)$ the undistorted true 3-D image;
- $h(x, y, z)$ the PSF of the imaging system;
- $n(x, y, z)$ the corrupting noise (assumed additive in our model).

In this notation, the coordinates (x, y) represent the discrete pixel spatial locations, z the slice location and $*$ designates the 3-D discrete linear convolution operator. The 3-D blind deconvolution problem consists then in determining $f(x, y, z)$ and $h(x, y, z)$ (or its inverse) given the blurred observation $g(x, y, z)$.

When the object to be recovered is imaged against a uniform or a noisy background, a commonly used method for solving the 2-D blind

Manuscript received May 4, 1999; revised October 7, 1999. This work was supported by the Institut National de la Recherche en Informatique et Automatique (INRIA), France through a postdoctoral grant. Asterisk indicates corresponding author.

*M. Mignotte is with the Institut National de Recherche en Informatique et Automatique, France, and the Département d'Informatique et de Recherche Opérationnelle, C. P. 6128, Succ. Centre-ville, Montréal, PQ H3C 3J7, Canada, (e-mail: mignotte@iro.umontreal.ca).

J. Meunier is with the Département d'Informatique et de Recherche Opérationnelle, Montréal, PQ H3C 3J7, Canada (e-mail: meunier@iro.umontreal.ca).
Publisher Item Identifier S 0018-9294(00)00892-2.

deconvolution problem consists in minimizing an error metric that optimizes the form of the restored image and the PSF (or its inverse) to fit the various constraints, *a priori* known, on the form of the solution; typically positivity and known support of the object. The steepest descent or conjugate gradient method are then generally used to achieve optimization [5], [6].¹ In our application, the true undistorted rCBF map of a human brain consists of a finite support imaged against a noisy background due to the Poisson noise phenomenon. In this section, we propose to find accurately this support thanks to an unsupervised 3-D Markovian segmentation technique and then to use a 3-D extension of such deconvolution technique for improving both spatial and interslice resolution of the SPECT volumes.

B. 3-D Extension of the NAS-RIF Algorithm

In the 3-D SPECT imagery context, the recent NAS-RIF algorithm [5] can be easily extended in order to take into account both the 2-D spatial and the interslice blur. We can derive a 3-D extension of this technique by simply considering a 3-D variable finite impulse response (FIR) filter $u(x, y, z)$ of dimension $N_{xu} \times N_{yu} \times N_{zu}$ with the blurred SPECT volume pixels $g(x, y, z)$ as input (see Fig. 1). The output of this filter gives an estimate of each cross-sectional 2-D true image $\hat{f}(x, y, z = k)$ (with $k \in [1, K]$ and K representing the number of transversal slices in the considered SPECT volume). Each resulting estimation is passed through a nonlinear filter which uses a nonexpansive mapping to project the estimated 2-D image into the space representing the known characteristics of the true image. The difference between this projected image $\hat{f}_{NL}(x, y, z = k)$ and $\hat{f}(x, y, z = k)$ is used as the error signal to update the variable filter $u(x, y, z)$. Fig. 1 gives an overview of the proposed 3-D-extended NAS-RIF deconvolution algorithm. Each cross-sectional 2-D image is assumed to be nonnegative with known support. The cost function used in the deconvolution procedure of the k th transversal 2-D image is defined as

$$J_k = \sum_{(x,y) \in \mathcal{D}_{[k]}} \hat{f}^2(x, y, z = k) \left(\frac{1 - \text{sgn}(\hat{f}(x, y, z = k))}{2} \right) + \sum_{(x,y) \in \overline{\mathcal{D}}_{[k]}} \left(\hat{f}(x, y) - L_B \right)^2 + \gamma \left(\sum_{\forall(x,y,z)} u(x, y, z) - 1 \right)^2$$

where $\hat{f}(x, y, z) = g(x, y, z) * u(x, y, z)$, and $\text{sgn}(f) = -1$ if $f < 0$ and $\text{sgn}(f) = 1$ if $f \geq 0$. $\mathcal{D}_{[k]}$ is the set of all pixels of $g(x, y, z = k)$ inside the region of support, and $\overline{\mathcal{D}}_{[k]}$ is the set of all pixels outside the region of support. The variable γ in the third term is nonzero only when L_B is zero, i.e., the background color is black. The third term is used to constrain the parameter away from the trivial all-zero global minimum for this situation. The authors have shown in [5] that the above equation is convex in the 2-D case with respect to u . This property remains true in the 3-D case so that convergence of the algorithm to the global minimum is ensured using the conjugate gradient minimization routine [5]. Let us note that a fully 3-D deconvolution scheme would consist in minimizing directly the cost function $J = \sum_{k=1}^K J_k$. Nevertheless, let us also notice that J_k and J being convex and the global minimum being ensured in both cases by the conjugate gradient optimization routine, the estimated solution (i.e., the SPECT volume given by minimizing J and the set of SPECT images given by minimizing each cost function J_k) are, thus, identical.

¹This class of methods has appeared more reliable in the SPECT image 2-D deconvolution context than the one called "grouped coordinate descent" that alternates between restoration of the image and PSF [7].

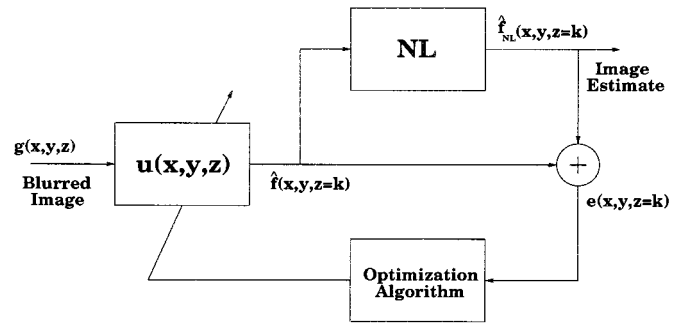


Fig. 1. Three-dimensional extension of the NAS-RIF deconvolution algorithm.

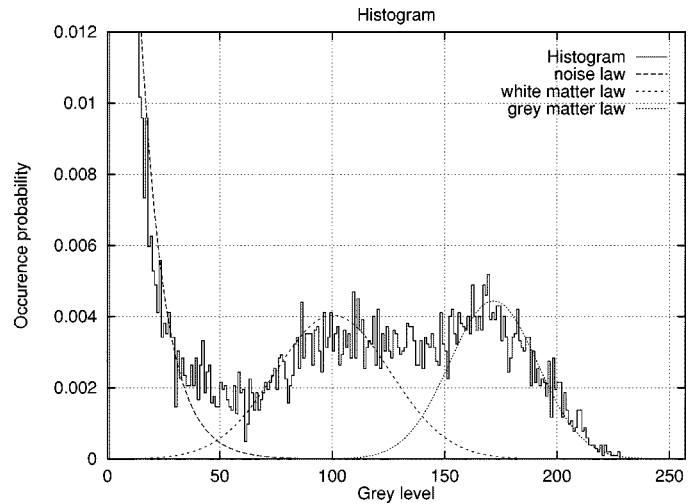


Fig. 2. Image histogram of the picture reported in Fig. 4 (solid curve) and estimated probability density mixture obtained with the iterative conditional estimation (ICE) procedure (dotted and dashed curves).

ICE Procedure			
$\Phi_{(e_1)}^{\text{final}}$	0.52(π)	11(α)	
$\Phi_{(e_2)}^{\text{final}}$	0.26(π)	100(μ)	648(σ^2)
$\Phi_{(e_3)}^{\text{final}}$	0.22(π)	172(μ)	383(σ^2)

Fig. 3. Estimated parameters for the SPECT volume reported in Fig. 4. π stands for the proportion of the three classes within the SPECT image. α are the exponential law parameter. μ and σ^2 are the Gaussian law parameters.

III. SUPPORT DETERMINATION METHOD

A. Introduction

In the 2-D case, the support can be roughly approximated by the smallest rectangle containing the entire object [5]. In order to automatically determine this rectangular frame, some of the proposed methods are based on hold-out methods [5], or inspired by the constraint assessment algorithm proposed in [8]. These methods are reliable for assessing the optimal 2-D rectangular support but cannot be easily extended in order to define a more accurate segmentation.

To this end, an alternative approach consists in exploiting the result of a 3-D unsupervised Markovian segmentation. Nevertheless, the problem of "unsupervised" Markovian segmentation is quite complex; the main difficulty is that the estimation of model parameters is required for the segmentation, while the segmentation result is needed

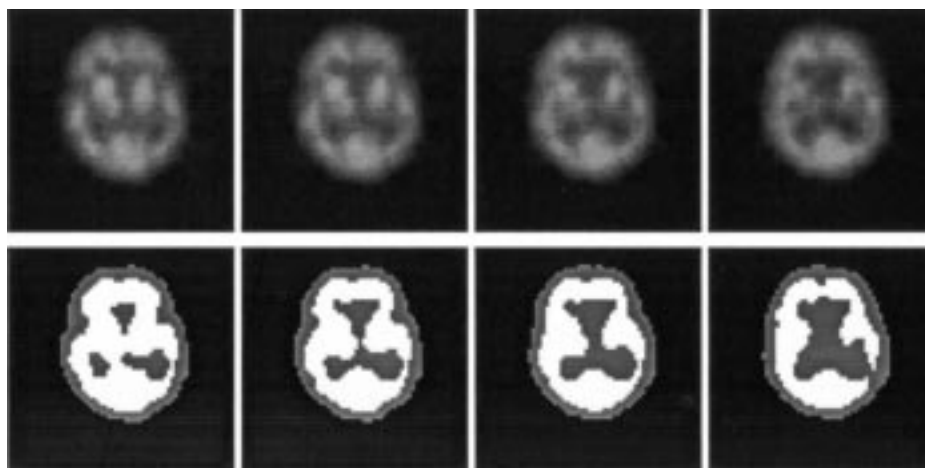


Fig. 4. Example of an unsupervised 3-D Markovian segmentation of a brain SPECT volume using the iterated conditional modes (ICM) deterministic relaxation technique and based on the parameters estimated by the ICE procedure. (top): Real brain SPECT volume (four central transversal slices) and (bottom) three-class Markovian segmentations.

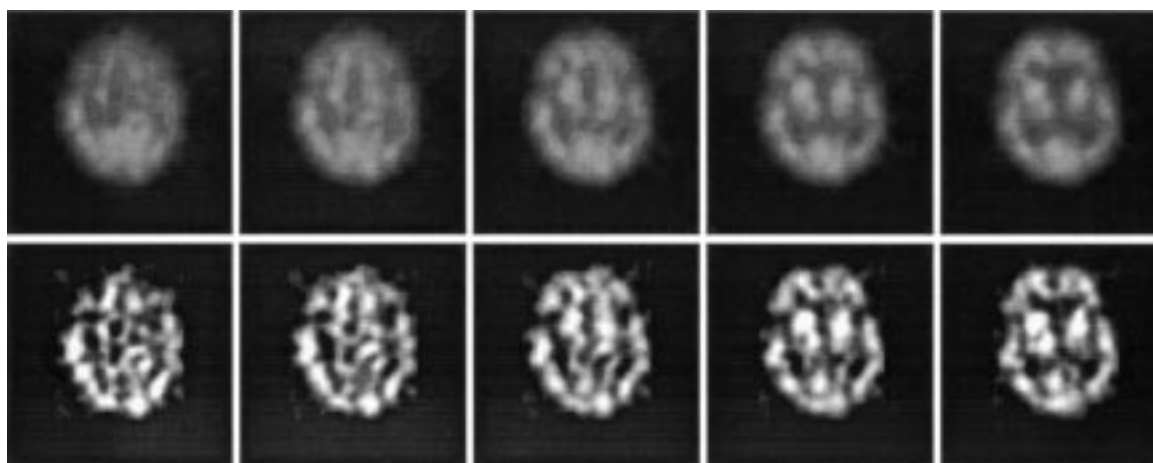


Fig. 5. Examples of human brain SPECT volume deconvolution given by the 3-D-extended version of the NAS-RIF algorithm combined with the Markovian segmentation-based support finding algorithm. (top) Five consecutive real cross-sectional SPECT slices and (bottom) deconvolution results.

for model parameter estimation. In order to solve this problem, a simple and reliable approach consists in having a two-step process. First, a parameter estimation step in which we have to estimate the MRF model parameter (i.e., the parameters of the grey level statistical distribution associated to each class of the SPECT volume). Then, a second step devoted to the segmentation itself based on the values of the estimated parameters.

B. 3-D Unsupervised Markovian Segmentation

We consider a couple of random fields $Z = (X, G)$, where $G = \{G_s, s \in S\}$ represents the field of observations located on the 3-D lattice S consisting of K lattices S_k of N sites s (associated to the N pixels of each transversal slice of the SPECT volume), and $X = \{X_s, s \in S\}$ the label field (related to the $K \times N$ class labels X_s of a segmented SPECT volume). Each aforementioned label is associated to a specific brain anatomical tissue or region of the SPECT volume; the cerebrospinal fluid “CSF” area designates the region that is normally due to the lack of radiations. In this distribution mixture parameter estimation and segmentation problems, this region designates the brain region filled with cerebrospinal fluid (without blood flow and,

thus, without radiation) and also the area outside the brain region. The “white matter” and “grey matter” (brightest region) are associated to a low and a higher level of blood flow, respectively [9]. Each G_s takes its value in $\{0, \dots, 255\}$ (256 grey levels), and each X_s in $\{e_1 = \text{“CSF”}, e_2 = \text{“white matter”}, \text{and } e_3 = \text{“grey matter”}\}$.

In the following, the parameters in upper-case letter designate the random variables whereas the lower-case letters represent the realizations of these concerned random variables. The distribution of (X, G) is defined, first, by prior distribution $P_X(x)$, supposed to be Markovian and second, by the site-wise conditional data likelihoods $P_{G_s/X_s}(g_s/x_s)$ whose shape and parameter vector $\Phi_{(x_s)}$ depends on the concerned class label x_s (g_s designates the grey level intensity associated to the site s). In order to take into account the Poisson noise phenomenon inherent to the SPECT imaging process in the “CSF” area, we model $P_{G_s/X_s}(g_s/e_1)$, by a exponential law [3] with parameter α , namely; $(1/\alpha) \exp[-(g_s/\alpha)]$. To describe the brightness within the “white matter” and the “grey matter” regions, we model the conditional density function for these two regions by two different Gaussian laws [3]. Finally, we assume independence between each random variable G_s given X_s . The observable G is called the “incomplete data” whereas Z constitutes the “complete data”.

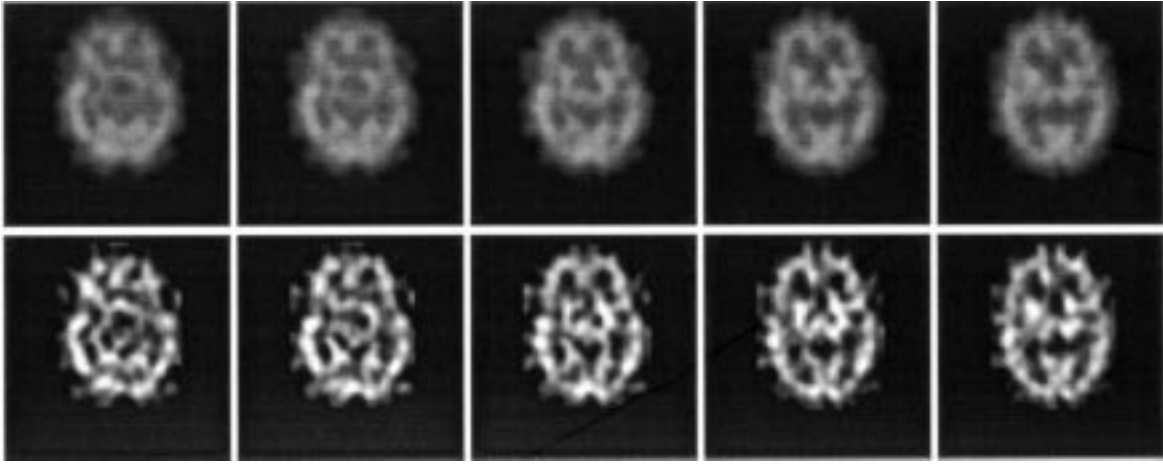


Fig. 6. Examples of human brain SPECT volume deconvolution given by the 3-D-extended version of the NAS-RIF algorithm combined with the Markovian segmentation-based support finding algorithm. (top) Five consecutive real cross-sectional SPECT slices and (bottom) deconvolution results.

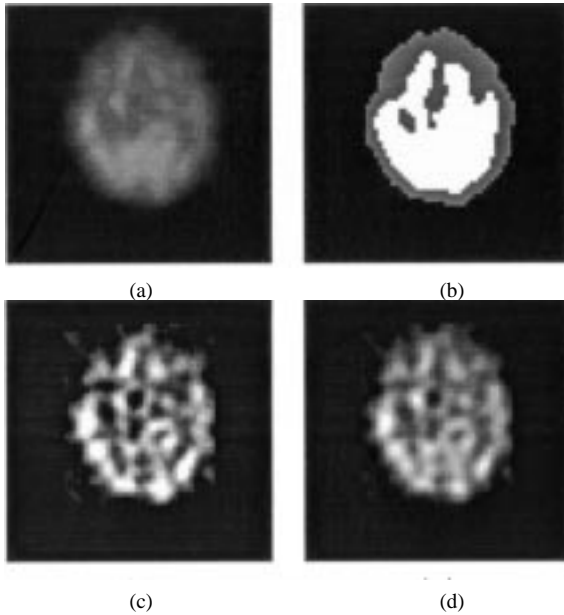


Fig. 7. Examples of human brain SPECT cross-sectional image segmentation and deconvolutions: (a) original SPECT cross-sectional human brain image, (b) unsupervised 3-D Markovian segmentation, (c) deconvolution result given by the 3-D-extended version of the NAS-RIF algorithm (inverse filter size is $3 \times 3 \times 3$), and (d) deconvolution result given by its 2-D version (inverse filter size is 5×5) [both deconvolution methods require the same computational load and are combined with the proposed Markovian segmentation-based support-finding algorithm (b)].

1) *Estimation Step*: In order to determine $\Phi = (\Phi_{(e_1)}, \Phi_{(e_2)}, \Phi_{(e_3)})$, we use the ICE algorithm. This estimation procedure [11] relies on an estimator $\hat{\Phi}(X, G)$ for completely observed data case. This iterative method starts from an initial parameter vector $\Phi^{[0]}$ (not too far from the optimal one) and generates a sequence of parameter vectors leading to the optimal parameters (in the least squares sense) with the following iterative scheme:

$$\Phi^{[p+1]} = \frac{1}{n} \left[\hat{\Phi}(x_{(1)}, g) + \cdots + \hat{\Phi}(x_{(n)}, g) \right]$$

where $x_{(i)}$, $i = 1, \dots, n$ are realizations of X drawn according to the posterior distribution $P_{X/G}(x/g, \Phi^{[p]})$. In order to decrease the

computational load, we can take $n = 1$ without altering the quality of the estimation [12]. Finally, we can use the Gibbs sampler algorithm [13] to simulate realizations of X according to the posterior distribution. For the local *a priori* model of the Gibbs sampler, we adopt a 3-D isotropic Potts model with a first-order neighborhood [10]. In this model, there are three parameters denoted $\beta_1, \beta_2, \beta_3$, called “the clique parameters” [10], and associated to the horizontal, vertical, and transverse binary cliques, respectively.² Given this *a priori* model, the prior distribution $P_X(x)$ can be written as

$$P_X(x) = \exp \left(- \sum_{\langle s, t \rangle} \beta_{st} (1 - \delta(x_s, x_t)) \right)$$

where summation is taken over all pairs of spatial and interlevel neighboring sites and δ is the Kronecker delta function. In order to favor homogeneous regions with no privileged orientation in the Gibbs sampler simulation process, we choose $\beta_{st} = \beta_1 = \beta_2 = \beta_3 = 1$. Finally, $\Phi^{[p+1]}$ is computed from $\Phi^{[p]}$ in the following way.

- Stochastic step*: Using the Gibbs sampler, one realization x is simulated according to the posterior distribution $P_{X/G}(x/g)$, with parameter vector $\Phi^{[p]}$.
- Estimation step*: The parameter vector $\Phi^{[p+1]}$ is estimated with the maximum likelihood (ML) estimator of the “complete data” corresponding to each class.

i) If $N_1 = \#\{s \in S: x_s = e_1\}$ is the number of pixels of the “CSF” area, the ML estimator $\hat{\Phi}_{(e_1)}$ of α is given by

$$[14]: \hat{\alpha}(x, g) = (1/N_1) \sum_{s \in S: x_s = e_1} g_s.$$

ii) If $N_2 = \#\{s \in S: x_s = e_2\}$ and $N_3 = \#\{s \in S: x_s = e_3\}$ pixels are located in the “white matter” and “grey matter” regions, respectively, the corresponding ML estimator of each class is given by the empirical mean and the empirical variance. For instance, for the “white matter” class, we have for $\hat{\Phi}_{(e_2)}$

$$\hat{\mu}(x, g) = \frac{1}{N_2} \sum_{s \in S: x_s = e_2} g_s$$

$$\hat{\sigma}^2(x, g) = \frac{1}{(N_2 - 1)} \sum_{s \in S: x_s = e_2} (g_s - \hat{\mu})^2$$

- Repeat until convergence is achieved; i.e., if $\hat{\Phi}^{[p+1]} \neq \hat{\Phi}^{[p]}$, we return to stochastic step.

²Cliques are subsets of sites which are mutual neighbors [10].

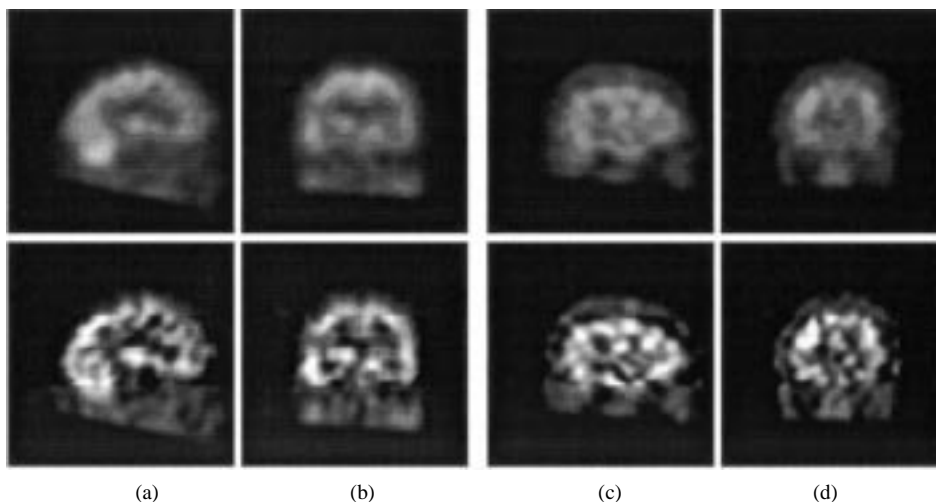


Fig. 8. Examples of (a), (c) sagittal and (b), (d) coronal sections of the (top) original and (bottom) deconvolved human brain SPECT volumes whose cross-sectional slices have been presented in Fig. 5 for (a) and (b) and in Fig. 6 for (c) and (d).

Fig. 2 represents the estimated distribution mixture of the SPECT volume shown in Fig. 4. The three site-wise conditional data likelihoods $P_{G_s/X_s}(g_s/e_k)$, $k = 1, 2, 3$ (weighted by the estimated proportion π_k of each class) are superimposed to the image histogram. Corresponding estimates obtained by the estimation procedure (requiring about ten iterations) are given in Fig. 3.

2) *Segmentation Step*: Based on the estimates given by the ICE procedure, we can compute an unsupervised 3-D Markovian segmentation of SPECT volumes. In this framework, the Markovian segmentation can be viewed as a statistical labeling problem according to a global Bayesian formulation in which the posterior distribution $P_{X/G}(x/g) \propto \exp -U(x, g)$ has to be maximized [10]. The corresponding posterior energy is

$$U(x, g) = \underbrace{\sum_{s \in S} -\ln P_{G_s/X_s}(g_s/x_s)}_{U_1(x, g)} + \underbrace{\sum_{\langle s, t \rangle} \beta_{st}(1 - \delta(x_s, x_t))}_{U_2(x)}$$

where

- U_1 adequacy between observations and labels;
- U_2 energy of the *a priori* model.

We use the deterministic ICM algorithm [10] to minimize this global energy function. For the initialization of this algorithm, we exploit the segmentation map obtained by a ML segmentation. Fig. 4 displays examples of unsupervised three-class segmentation, exploiting parameters estimated with the ICE procedure. In this segmentation, the “CSF”, the “white matter” and the “grey matter” are represented by a dark, a grey, and a white region, respectively, in order to visually express the activity level of the blood flow. The support \mathcal{D} is then determined simply by the set of pixels belonging to the white and grey matter classes.

IV. EXPERIMENTAL RESULTS

The effectiveness of this 3-D blind deconvolution method was tested on several SPECT volumes composed of 64 transversal slices of 64×64 pixels with 256 grey levels. Those presented in this section are only a few examples.

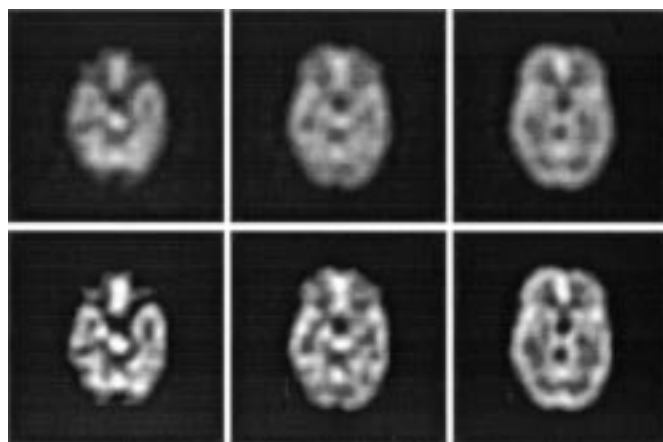


Fig. 9. Examples of deconvolution obtained by our 3-D blind deconvolution approach on some cross-sectional slices of a SPECT phantom. Top: real cross-sectional SPECT phantom slices. Bottom: deconvolution results.

The initial inverse FIR filter required by the NAS-RIF algorithm is the Kronecker delta function [5] and the size of this inverse filter is $3 \times 3 \times 3$ pixels. Besides, we have used $\gamma = 0$ because the background of SPECT images is not completely black. We recall that the object support determination is based on the result of the 3-D unsupervised Markovian segmentation (see Section III). Finally, in order to objectively compare the resolution improvements between the original and deconvolved SPECT volumes, we have decided to stretch the histogram of the estimated 3-D volume at convergence (i.e., $\hat{f}_{\text{final}}(x, y, z)$) in order to get the same mean value as the original input SPECT volume $g(x, y, z)$. The computational cost for a blind deconvolution cross-sectional image is about 50 s on a standard SunSparc 2 workstation (20 s for the support determination of the whole volume and 30 s for the blind deconvolution of each cross-sectional image).

Figs. 5 and 6 present examples of brain SPECT volume deconvolutions obtained by this 3-D blind deconvolution approach. The algorithm (requiring about 250 iterations) converges to a very good estimate of the solution without *a priori* information on the PSF and allows to noticeably improve the resolution of the original SPECT volume. For instance, this restoration procedure allows efficiently to detect small localized singularities associated with lesion or tumors that may not be



Fig. 10. Examples of some consecutive cross-sectional slices of the segmented phantom (ground truth).

clearly visible in the original blurred image. Fig. 7(c) and (d) shows the resolution improvement obtained by the 3-D-extended version of the NAS-RIF algorithm over its 2-D version for a given cross-sectional image (both methods are combined with the proposed unsupervised Markovian segmentation-based support-finding algorithm). The resolution improvement is visible (although difficult to appreciate due to the diffusive effect of the printer) and can be clearly noticed on a computer screen. Fig. 8 shows examples of sagittal and coronal sections of the original and deconvolved human brain SPECT volumes whose cross-sectional slices have been presented in Figs. 5 and 6. The improvement of the interslice resolution is also clearly visible.

The effectiveness of this deconvolution technique is also tested on a real SPECT phantom (i.e., a physical Plexiglas head phantom filled with radioactive material and measured by a SPECT system) for which the ground truth of this segmented phantom is exactly known and, thus, for which the performance of our proposed method can then be objectively judged. Fig. 9 presents examples of brain SPECT volume deconvolutions obtained by our 3-D blind deconvolution approach on this SPECT phantom. We can easily notice that this SPECT volume is less noisy and less blurred than the real human brain SPECT volumes previously presented and processed (due to several factors such as a different dose of radioactive isotopes contained in each uniform region of this SPECT phantom, a longer acquisition time, the stillness of this simulated brain during the SPECT process, reduced attenuation, etc.) Nevertheless, once again, the resolution improvement remains visible.

In order to fully assess the success of this restoration procedure, we use the specific evaluation criteria proposed in [4], based on the estimation of the three following measures:

- 1) First, the average contrast of the image, defined by $C = (1 - m_2/m_3)$, where m_2 and m_3 are the mean of the pixel value in the "white matter" and "grey matter" area, respectively.
- 2) Second, the image mottle M_2 in the "white matter" region, characterized by taking the ratio of the standard deviation σ_2 of pixel values in this area to the mean m_2 .
- 3) Third, the image mottle M_3 in the "grey matter" area.

These two last parameters allow to measure the amplification of the noise and/or measure the presence of undesirable artifacts that can be created by the deconvolution procedure in a uniform region of the real SPECT phantom (thus with ideally uniform radioactive activity). Due to the difference of proportion of pixels belonging to each brain anatomical tissue, we consider the total mottle measure given by $M = \rho_2 M_2 + \rho_3 M_3$, with ρ_2 and ρ_3 designates the proportion of pixel belonging to the "white matter" and "gray matter" area, respectively. A reliable SPECT image restoration technique will then allow to enhance the contrast of the image with little increase in mottle, i.e., without amplifying too much the noise and/or without creating false artificial features (technically, an increase by a factor of 1.1–1.2 of the original mottle of the image remains acceptable if the contrast enhancement is significantly increased [4]). Due to the difference of thickness between the cross-sectional slices of the real and segmented phantom, these

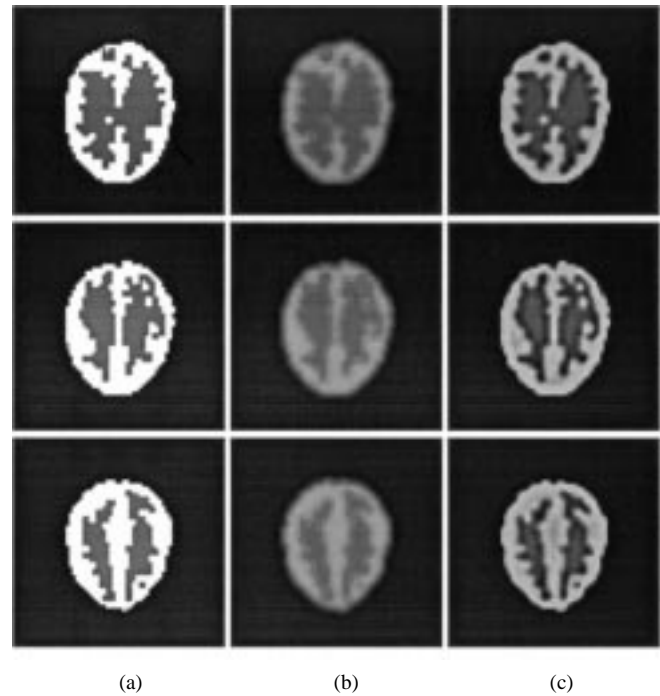


Fig. 11. Example of deconvolution results on some cross-sectional slices of a synthetic SPECT volume: (a) ground truth of the segmented synthetic slices, (b) synthetic SPECT slices, and (c) deconvolution results.

above mentioned measures are estimated on the whole 3-D phantom after this one has been registered [15] on the ground truth of the segmented phantom volume (see Fig. 10 where some consecutive slices of the segmented phantom are shown). Our proposed restoration technique allows a contrast enhancement from 9% to 21% between the original and deconvolved SPECT phantom along with an acceptable amplification of the mottle of this 3-D image by a factor of 1.18 (from 17% to 20%). This represents a significant improvement in image quality with a very small penalty and attest the validity of our restoration method. Let us add that the registration process [15] induces most probably artificial features and our real restoration results are most likely better.

Finally, we have also tested our 3-D deconvolution technique on some cross-sectional slices of a synthetic SPECT volume. In order to simulate at best the typical characteristics of real human brain SPECT images, we have re-created three homogeneous regions and added the corresponding noise for each ones, according to the grey level statistical distribution already estimated on a real human brain SPECT volume (see the distribution mixture presented in Fig. 2 and parameters given in Fig. 3). We have also added a 3-D Gaussian blur in order to simulate the 3-D scattering of the emitted photons. Fig. 11 shows the ground truth of the segmented synthetic slices, the synthetic SPECT slices and finally

the deconvolution results obtained by our restoration method. The resolution improvement is visible and the proposed procedure allow efficiently to recover high frequencies of the undistorted (nonconvolved) image.

V. CONCLUSION

In this paper, we have shown that a 3-D extension of the NAS-RIF deconvolution procedure noticeably improves the resolution of human brain 3-D SPECT images and can be a great help to facilitate their interpretation by the nuclear physician. We have also shown that this 3-D blind deconvolution technique gives superior performance than its 2-D version and can efficiently exploit the result of a 3-D unsupervised Markovian segmentation in order to find the exact support of the object to be restored. This segmentation allows to accurately fit the finite-support constraint of this optimization strategy-based deconvolution technique. Finally, this 3-D blind deconvolution technique combined with the unsupervised segmentation leads to a restoration procedure that is completely data driven and really compatible with an automatic processing of massive amounts of 3-D SPECT data.

ACKNOWLEDGMENT

The authors would like to thank J.-P. Soucy and C. Janicki of the Centre Hospitalier de l'Université de Montréal (CHUM), Montréal, Canada, for providing the SPECT images.

REFERENCES

- [1] D. Boulfelfel, R. M. Rangayyan, L. J. Han, and R. Kloiber, "Preconstruction restoration of myocardial single photon emission computed tomography images," *IEEE Trans. Med. Imag.*, vol. 11, pp. 336–341, June 1992.
- [2] M. T. Madsen and C. H. Park, "Enhancement of SPECT images by Fourier filtering the projection set," *J. Nucl. Sci.*, vol. 26, pp. 2687–2690, 1979.
- [3] T. S. Curry, J. E. Dowdey, and R. C. Murry, *Christensen's Physics of Diagnostic Radiology*. Philadelphia, PA: Lea & Febiger, 1990.
- [4] S. Webb, A. P. Long, R. J. Ott, M. O. Leach, and M. A. Flower, "Constrained deconvolution of SPECT liver tomograms by direct digital image restoration," *Med. Phys.*, vol. 12, no. 1, pp. 53–58, 1985.
- [5] D. Kundur and D. Hatzinakos, "Blind image restoration via recursive filtering using deterministic constraints," in *Proc. Int. Conf. Acoustics Speech, and Signal Processing*, vol. 4, 1996, pp. 547–549.
- [6] Y. L. You and M. Kaveh, "A regularization approach to joint blur identification and image restoration," *IEEE Trans. Image Processing*, vol. 5, pp. 416–428, Mar. 1996.
- [7] M. Mignotte and J. Meunier, "A comparison of supervised and blind deconvolution techniques applied in SPECT imagery," Département d'informatique et de recherche opérationnelle (DIOR), Université de Montréal, Montréal, PQ, Canada, , Tech. Rep., April 1999.
- [8] S. J. Reeves and M. Mersereau, "Automatic assessment of constraint sets in image restoration," *IEEE Trans. Image Processing*, vol. 1, pp. 119–123, Jan. 1992.
- [9] D. C. Costa and P. J. Ell, *Brain Blood Flow in Neurology and Psychiatry*, P. J. Ell, Ed. London, U.K.: Churchill Livingstone, 1991.
- [10] J. Besag, "On the statistical analysis of dirty pictures," *J. Roy. Stat. Soc.*, vol. B-48, pp. 259–302, 1986.
- [11] F. Salzenstein and W. Pieczynski, "Unsupervised Bayesian segmentation using hidden Markovian fields," in *Proc. Int. Conf. Acoustics, Speech, and Signal Processing*, May 1995, pp. 2411–2414.
- [12] B. Braathen, P. Masson, and W. Pieczynski, "Global and local methods of unsupervised Bayesian segmentation of images," *Graphics Vision*, vol. 2, no. 1, pp. 39–52, 1993.
- [13] S. Geman and D. Geman, "Stochastic relaxation, Gibbs distributions and the Bayesian restoration of images," *IEEE Trans. Pattern Anal. Machine Intell.*, vol. 6, pp. 721–741, Nov. 1984.
- [14] S. Banks, *Signal Processing, Image Processing and Pattern Recognition*. Englewood Cliffs, NJ: Prentice-Hall, 1990.
- [15] K. J. Friston, J. Ashburner, C. D. Frith, J. B. Poline, J. D. Heather, and R.S.J. Frackowiak, "Spatial registration and normalization of images," *Human Brain Mapping*, vol. 3, no. 3, pp. 165–189, 1995.